Magnetic structure of strontium ferrite $Sr_4Fe_4O_{11}$

2003 J. Phys.: Condens. Matter 15 8691

(http://iopscience.iop.org/0953-8984/15/50/003)

INSTITUTE OF PHYSICS PUBLISHING JOURNAL OF PHYSICS: CONDENSED MATTER

J. Phys.: Condens. Matter **15** (2003) 8691–8701 PII: S0953-8984(03)68620-0

Magnetic structure of strontium ferrite $Sr_4Fe_4O_{11}$

M Schmidt[1,2,5], **M Hofmann**[3] **and S J Campbell**[4,3]

[1] ISIS Facility, Rutherford Appleton Laboratory, Chilton, Didcot, Oxon OX11 0QX, UK
[2] Department of Physics and Astronomy, Michigan State University, East Lansing, USA
[3] Technische Universität München, ZWE, FRM-II 85747 Garching, Germany
[4] School of Physical, Environmental and Mathematical Sciences, The University of New South Wales, Australian Defence Force Academy, Canberra, ACT 2600, Australia

E-mail: M.Schmidt@rl.ac.uk

Received 4 September 2003
Published 3 December 2003
Online at stacks.iop.org/JPhysCM/15/8691

Abstract

The crystal and magnetic structure of strontium ferrite $Sr_4Fe_4O_{11}$ ($SrFeO_{2.75}$) has been investigated using neutron powder diffraction and magnetic susceptibility measurements over the temperature range 1.5–293 K and by Mössbauer spectroscopy at room temperature. $Sr_4Fe_4O_{11}$ is orthorhombic (symmetry group *Cmmm*) over the temperature range 1.5–293 K. Its crystal structure contains two iron sites occupied by trivalent and tetravalent iron. The trivalent magnetic moments order antiferromagnetically below $T_N = 232(4)$ K and the magnetic unit cell coincides with the chemical cell. The ordered moments are parallel to the *b* axis and the tetravalent iron moments form a magnetically frustrated sublattice. The extrapolated value of the Fe^{3+} moment is 3.55(5) μ_B at 0 K. The antiferromagnetic coupling occurs by the superexchange mechanism and is mediated by oxygen ions. There are no signs of long-range magnetic order in the tetravalent sublattice down to 1.5 K.

1. Introduction

Despite the apparent simplicity of the $SrFeO_x$ system, it is structurally complex with a range of subtle structures and transformations taking place on variation of the oxygen content ($2.5 \leqslant x \leqslant 3.0$). Adding to the interest, the $SrFeO_x$ system has been shown to exhibit a variety of physical and chemical properties that change over broad ranges of temperatures, oxygen partial pressure and magnetic field. The compound contains a mixture of iron in trivalent and tetravalent states. At elevated temperatures ($T > 473$ K) $SrFeO_x$ forms a cubic solid solution of its compositional end members $SrFeO_3$ ($x = 3$) and $Sr_2Fe_2O_5$ ($x = 2.5$). The composition x and the crystal structure of $SrFeO_x$ are functions of temperature and oxygen partial pressure. This high-temperature $SrFeO_x$ phase exhibits charge disorder in the iron site and vacancy disorder in the oxygen site [1–7]. In addition, the high-temperature phase

[5] Author to whom any correspondence should be addressed.

0953-8984/03/508691+11$30.00

of $SrFeO_x$ exhibits substantial electronic and ionic conductivities. Materials derived from $SrFeO_x$ are considered to be suitable for use in oxygen conducting devices such as electrodes in solid oxide fuel cells (SOFCs) or oxygen conducting membranes in pressure driven oxygen generators or in partial oxidation reactors [8, 9].

The crystal structures of $SrFeO_x$ with different oxidation states of iron and oxygen vacancies are found to order with decrease in temperature and, depending on the oxygen content, $SrFeO_x$ forms one of four different phases: $SrFeO_3$, $Sr_8Fe_8O_{23}$ ($x = 2.875$), $Sr_4Fe_4O_{11}$ ($x = 2.75$) and $Sr_2Fe_2O_5$ ($x = 2.5$). For intermediate compositions $SrFeO_x$ forms a mixture of two neighbouring phases [2, 7, 10, 11]. These low-temperature phases exhibit interesting magnetic properties, and materials with oxygen stoichiometry $x = 2.95$ have been found to exhibit a large magnetoresistance effect [12, 13].

The $Sr_4Fe_4O_{11}$ phase, which contains equal numbers of iron atoms in tetravalent and trivalent states, was first reported by Tofield *et al* [14]. However, its room-temperature crystal structure remained undecided and has only recently been solved by Hodges *et al* [11]. In this paper we report the results of a powder neutron diffraction study of the $Sr_4Fe_4O_{11}$ phase over the temperature range 1.5–293 K. The neutron studies are supported by magnetic susceptibility and Mössbauer effect measurements. We describe the evolution of the $Sr_4Fe_4O_{11}$ crystal structure with temperature and propose a model which describes the magnetic order in this phase. We discuss the relationship between the crystal structure and the magnetic properties of $Sr_4Fe_4O_{11}$.

2. Experimental details

The $Sr_4Fe_4O_{11}$ ($SrFeO_{2.75}$) sample was prepared from a mixture of haematite (Fe_2O_3, 99.9% purity from Electronic Space Product International) and strontium carbonate ($SrCO_3$, 99.9+% purity from Aldrich) combined in the molar ratio 1:2 respectively. The mixture was ball milled for 12 h and then fired on an alumina combustion boat at 1373 K in air for total of 55 h. During the procedure the sinter was ground and analysed for traces of transient phases using x-ray powder diffraction. Once the impurity phases disappeared the sample was fired at 1473 K for 8 h in air and cooled to room temperature. $SrFeO_x$ prepared in this way is found to be oxidized to the composition $x = 2.81$; its oxygen content was adjusted to $x = 2.75$ by annealing at 838 K in flowing air for 24 h. The air atmosphere was then quickly replaced by argon and the sample withdrawn from the hot zone before being allowed to cool in argon [15]. The oxygen stoichiometry of the ferrite was confirmed to be $x = 2.753$ by mass loss upon reduction to $Sr_2Fe_2O_5$ in a thermogravimetric analyser. This oxygen stoichiometry value indicates slight Fe^{4+} excess in the sample.

The ^{57}Fe Mössbauer measurements were carried out at room temperature using a standard spectrometer and a ^{57}Co/Rh source. A thin layer of $Sr_4Fe_4O_{11}$ powder was spread on to sticky tape and the data from this sample collected over a period of one week. The spectrometer was calibrated using a standard α-Fe foil with isomer shift values quoted relative to the centre of the α-Fe spectrum.

The neutron powder diffraction experiments were carried out at BENSC, at the Hahn–Meitner Institut in Berlin. The sample was placed in a standard helium cryostat and the measurements carried out over the temperature range 1.5–293 K. The diffraction data were collected using the E6 focusing diffractometer and a neutron wavelength of 2.447 Å over the angular range 5°–105°. The diffraction patterns were analysed using the GSAS program suite [16].

The magnetic susceptibility of $Sr_4Fe_4O_{11}$ was measured using a SQUID magnetometer over the temperature range 5–299 K by cooling the sample in both zero field (ZFC) and in a magnetic field of 100 Oe (FC).

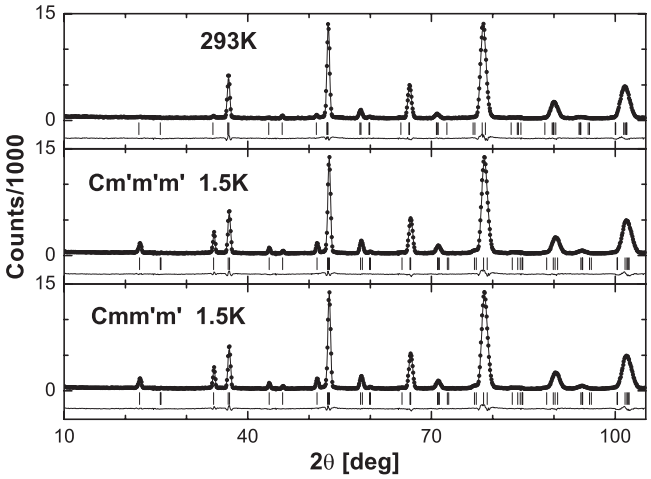

Figure 1. Neutron diffraction patterns of $Sr_4Fe_4O_{11}$ at 293 and 1.5 K. The 293 K pattern was refined in the *Cmmm* space group. As discussed in the text the magnetically ordered 1.5 K pattern was refined using $Cm'm'm'$ and $Cmm'm'$ Shubnikov groups. The circles represent the observed intensities; the solid curves are the calculated spectra and the difference curves. The vertical strokes mark the nuclear and magnetic Bragg reflections.

3. Results and discussion

3.1. Crystal structure

Figure 1 shows the neutron diffraction patterns for $Sr_4Fe_4O_{11}$ at room temperature and 1.5 K. $Sr_4Fe_4O_{11}$ was found to be orthorhombic over the entire temperature range of 1.5–300 K with no evidence of a structural transformation. The crystal structure of $Sr_4Fe_4O_{11}$ is consistent with the model published by Hodges *et al* [11]. Comparison of the two diffraction patterns shows a clear increase of intensity of some diffraction lines due to magnetic scattering in the 1.5 K pattern (e.g. (110), (111), (310) and (311) at $2\theta = 22.4°$, 34.5°, 43.4° and 51.3° respectively). All of the diffraction patterns of $Sr_4Fe_4O_{11}$ in the paramagnetic state were well refined using the *Cmmm* symmetry group. The presence of magnetic reflections become apparent in the pattern collected at 200 K and the results of the refinements are presented in table 1. It should be noted that the relatively long neutron wavelength of 2.447 Å was used to aid investigation of the magnetic scattering. Results were therefore obtained over a relatively narrow Q range (0.22–4.07 $Å^{-1}$), which in turn made it difficult to obtain reliable values of the Debye–Waller factors (the maximum value of $(\sin\theta/\lambda)^2$ was only 0.11). The temperature factors were freely refined, but some of them were found to become smaller than their standard deviation. On average the Debye–Waller factors were equal to approximately 0.005 $Å^2$ for Fe and Sr and 0.01 $Å^2$ for oxygen atoms.

The lattice constants of $Sr_4Fe_4O_{11}$ were found to increase monotonically with temperature and the lattice expansion is well described by a parabolic function. This behaviour is consistent with the absence of any structural transition in the $Sr_4Fe_4O_{11}$ over this temperature range.

The crystal structure of $Sr_4Fe_4O_{11}$ at 1.5 K is presented in figure 2 using Fe–O polyhedra. There are two iron sites in the $Sr_4Fe_4O_{11}$ crystal structure and they form alternating layers perpendicular to the c axis. The Fe(1) iron site has a five-coordinated local environment and the Fe(2) iron is located in octahedral surroundings (here we follow the atom-labelling scheme of Hodges *et al* [11]). The five-coordinated environment of Fe(1) is formed by one O(1)

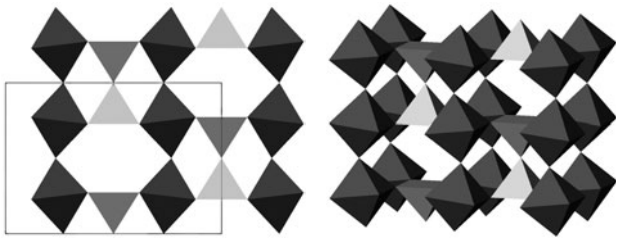

Figure 2. Views of the $Sr_4Fe_4O_{11}$ crystal structure at 1.5 K along the [001] direction (left) and the same structure slightly inclined (right). The structure is visualized using the five-coordinated Fe(1) pyramids and the Fe(2) octahedra (the Sr atoms are not shown for clarity). The pyramids form the 'bowtie' units by sharing an O(1) atom. Note the tilting of the Fe(2) octahedra introduced by pairs of the pyramidal sites. The a and b orthorhombic axes are horizontal and vertical in the pictures respectively. The rectangle outlines the unit cell.

Table 1. Structural parameters for $Sr_4Fe_4O_{11}$ refined in space group $Cm'm'm'$ in the temperature range of 1.5–200 K and in space group $Cmmm$ at 249 and 293 K. Sr(1) 2c (1/2, 0, 1/2); Sr(2) 2d(0, 0, 1/2); Sr(3) 4g (x, 0, 0); Fe(1) 4i(1/2, y, 0); Fe(2) 4f (1/4, 1/4, 1/2); O(1) 2b (1/2, 0, 0); O(2) 4h (x, 0, 1/2); O(3) 16r (x, y, z); $Z = 2$.

T (K)	a (Å)	b (Å)	c (Å)	Sr(3) x	Fe(1) y	O(2) x		
1.5	10.943(1)	7.6795(4)	5.4549(6)	0.260(1)	0.241(2)	0.268(1)		
30	10.944(1)	7.6799(4)	5.4551(6)	0.260(1)	0.242(2)	0.268(1)		
70	10.945(1)	7.6808(4)	5.4553(6)	0.259(1)	0.243(2)	0.268(1)		
100	10.945(1)	7.6820(4)	5.4556(6)	0.259(1)	0.240(2)	0.267(1)		
150	10.947(1)	7.6858(4)	5.4588(7)	0.259(1)	0.242(2)	0.268(1)		
200	10.950(2)	7.6894(4)	5.4605(8)	0.259(1)	0.242(2)	0.269(1)		
249	10.954(2)	7.6942(4)	5.4635(9)	0.2579(9)	0.243(2)	0.269(1)		
293	10.958(2)	7.6994(4)	5.4659(9)	0.2571(9)	0.245(1)	0.269(1)		
T (K)	O(3) x	O(3) y	O(3) z	Fe(1) m_y (μ_B)	R_{wp}	R_p	χ^2	R_p ($-Bknd$)
1.5	0.381(2)	0.2726(7)	0.241(3)	3.55(5)	0.077	0.054	5.272	0.043
30	0.381(1)	0.2731(7)	0.239(3)	3.57(5)	0.077	0.053	5.254	0.041
70	0.381(2)	0.2737(7)	0.239(3)	3.49(5)	0.077	0.054	5.262	0.043
100	0.381(1)	0.2728(7)	0.240(3)	3.29(5)	0.076	0.054	5.155	0.043
150	0.381(1)	0.2732(7)	0.240(3)	2.83(5)	0.076	0.053	5.100	0.042
200	0.381(1)	0.2733(7)	0.241(3)	1.93(6)	0.076	0.053	5.089	0.040
249	0.381(1)	0.2746(6)	0.239(3)	—	0.076	0.053	5.008	0.041
293	0.381(1)	0.2741(6)	0.239(3)	—	0.076	0.052	4.822	0.039

and four O(3) atoms, which form the base of a pyramid. The O(1) atom is shared by two neighbouring Fe(1) sites and forms a 'bowtie' unit. The Fe(1) atom is located close to the base of the pyramid. The octahedral surroundings of Fe(2) are formed by two O(2) and four O(3) atoms. The pyramids and octahedra share the O(3) atoms.

The Fe–O bond lengths are shown in figure 3 as a function of temperature. The Fe(2)–O(2) bond (∼1.93 Å) shows a slight tendency to increase with temperature whereas the Fe(2)–O(3) bond (∼2.03 Å) is found to be constant within the experimental error. The corresponding angles O(2)–Fe(2)–O(3) and O(3)–Fe(2)–O(3) were found to be constant and close to 90°. The resulting Fe(2) octahedron is compressed but its shape and size remains essentially the same down to 1.5 K. The Fe(2)–O(2) bonds form a zigzag with Fe(2)–O(2)–Fe(2) = 168.4(9)° at 1.5 K, 167.4(7)° at 293 K and O(2)–Fe(2)–O(2) = 180° angles (fixed by symmetry). This

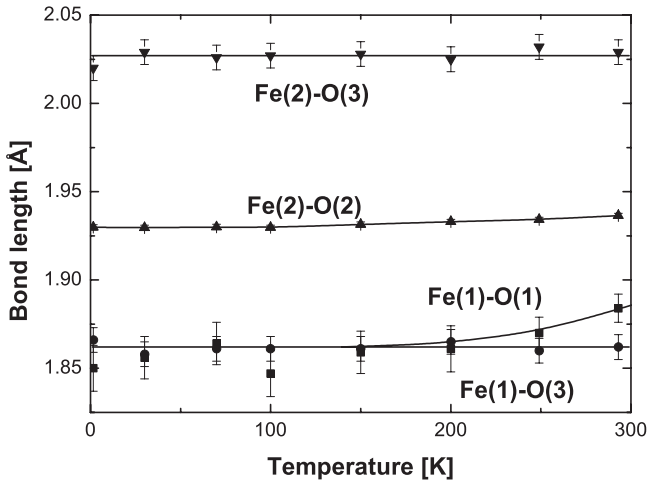

Figure 3. The Fe–O bond lengths in $Sr_4Fe_4O_{11}$ as a function of temperature. The lines act as guides to the eye.

zigzag is a result of a structural distortion introduced by the pyramid 'bowties' (see figure 2) placed in spaces between every four octahedron chains running along the *b* axis. However, the distortion causes only tilting of the octahedrons and does not change their shape (see figure 2). Within the experimental error the Fe(1)–O(3) bond ($\sim$1.86 Å) remains unchanged with temperature; the Fe(1)–O(1) bond equals the Fe(1)–O(3) bond up to $\sim$200 K, increasing above this temperature. The O(1)–Fe(1)–O(3) angle equals 97.4(4)° at 200 K and 97.0(3)° at 293 K. As a result the Fe(1) atom moves away from the O(1) atom towards the base of the pyramid with increasing temperature.

3.2. Mössbauer spectroscopy

The room-temperature Mössbauer spectrum of $Sr_4Fe_4O_{11}$ presented in figure 4 exhibits the same overall spectral shape as observed in earlier studies. However, whereas previous results were analysed assuming that there are more than two iron sites in the Mössbauer spectrum of $Sr_4Fe_4O_{11}$ [2, 10, 17, 18], the present results have been analysed on the basis of two iron sites. Consistent with the recent crystallographic study [11], the two iron sites are expected to be populated equally. The spectrum was initially fitted with three Lorentzian lines to characterize the three dominant resonance features. The three absorption lines were found to have equal widths and intensity ratios of 2:1:1. Given that neither of the iron sites in $Sr_4Fe_4O_{11}$ has a local cubic environment, both sites are expected to produce an electric field gradient and thus a quadrupole doublet in the Mössbauer spectrum. The spectrum was therefore fitted using two doublets; this led to the subspectral components shown in figure 4 and Mössbauer hyperfine parameters listed in table 2. As shown in table 2, site B has a small negative isomer shift and exhibits moderate quadrupole splitting (QS) compared with site A. The isomer shift of site B is characteristic of tetravalent iron in the high-spin state ($S = 2$) while the isomer shift of site A is characteristic of trivalent iron [19]. The results of the fitting (table 2) indicates that the fraction of the B sites slightly exceeds 50%, which is consistent with the slight oxygen excess in the sample.

The low-temperature Mössbauer spectra of $Sr_4Fe_4O_{11}$ published by Gibb [17] indicate that only Fe^{3+} in $Sr_4Fe_4O_{11}$ exhibits magnetic ordering below 220 K. The published hyperfine field

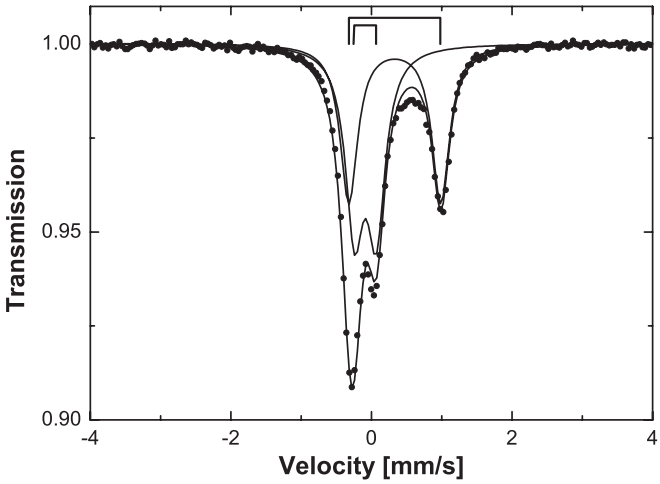

Figure 4. The Mössbauer spectrum of $Sr_4Fe_4O_{11}$ at room temperature. The solid curves show the final fit to the data points along with the resultant spectral components as discussed in the text. The line positions of the doublets are indicated by the stick diagrams.

Table 2. Refined parameters of $Sr_4Fe_4O_{11}$ Mössbauer spectrum at room temperature. The numbers in parentheses denote the standard deviation of the fit.

Site	IS (mm s^{-1})	QS (mm s^{-1})	Fraction (%)
A	0.332(2)	1.307(4)	47
B	−0.087(2)	0.311(3)	53

values for $Sr_4Fe_4O_{11}$ of $B_{hf} \sim 46$ T are in the range characteristic for ordered Fe^{3+} magnetic moments [2, 10, 17]. The Fe^{4+} iron in the low-temperature Mössbauer spectra of $Sr_4Fe_4O_{11}$ produces only a broad peak centred around 0 mm s^{-1}, with this behaviour persisting down to 4.2 K [2, 10, 17]. The broad peak indicates a distribution of spectral parameters with no sign of short- or long-range magnetic ordering for the Fe^{4+} iron.

3.3. Magnetic susceptibility

Figure 5 shows the molar magnetic susceptibility of $Sr_4Fe_4O_{11}$ as a function of temperature. The magnetic susceptibility of $Sr_4Fe_4O_{11}$ is relatively small (note that the zero-field-cooled (ZFC) susceptibility curve of $Sr_4Fe_4O_{11}$ in figure 5 is scaled up by $\times 50$). The ZFC susceptibility curve increases slightly with decreasing temperature, exhibiting a peak at 232 K. As discussed below, this is identified as the Néel temperature $T_N = 232$ K. The susceptibility then decreases at an increasing rate before becoming negative below 65 K. This behaviour is most likely due to ions with filled electronic shells as the absolute value of the magnetic susceptibility of $Sr_4Fe_4O_{11}$ is very small indeed for an iron compound. The shape of the ZFC curve around the peak is characteristic of an antiferromagnet–paramagnet phase transition and is consistent with previous Mössbauer findings [2, 10, 17] and the present neutron diffraction measurements. The susceptibility curve above 232 K obeys the Curie–Weiss law $\chi(T) = C/(T + \theta)$ with $\theta = -598(9)$ K. The values of the FC susceptibility curve of $Sr_4Fe_4O_{11}$ are equal to the ZFC values from 299 K down to 232 K before increasing with decreasing temperature. The FC susceptibility appears to saturate around 5 K.

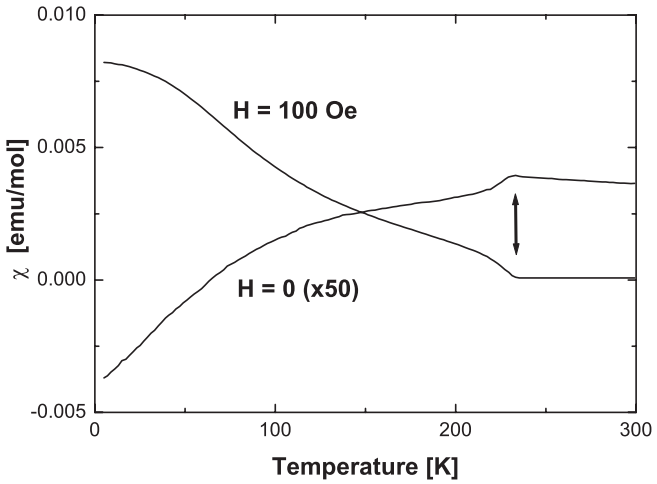

Figure 5. Molar magnetic susceptibility of $Sr_4Fe_4O_{11}$ as a function of temperature. The data were obtained by zero-field cooling (ZFC) and by cooling in a field (FC) of 100 Oe (note that the data in the zero-field curve have been multiplied by 50). The peak in the ZFC and the upturn in the FC susceptibility occur at 232 K as indicated by the arrows.

The difference in the FC and ZFC susceptibility curves below $T_N = 232$ K indicates additional magnetization below the Néel point with the FC susceptibility being almost two orders of magnitude greater than the zero-field susceptibility. The applied magnetic field is likely to have caused a partial alignment of the tetravalent iron magnetic moments. However, the effect of these magnetic moments vanishes when the sample becomes paramagnetic. This is an indication that electrons of tetravalent iron become localized below the Néel point while the trivalent spins undergo magnetic ordering.

3.4. Magnetic structure

As discussed above, Mössbauer measurements indicate that only one Fe sublattice orders magnetically. The observed magnetic reflections in the neutron diffraction patterns (see figure 1) can be successfully fitted using two magnetic models. These models are very similar to each other since the sublattices of the Fe(1) and Fe(2) atoms are almost identical. The only difference—except for the oxygen surroundings—is their spacing along the *b* axis. These models can be described using the $Cm'm'm'$ and $Cmm'm'$ Shubnikov groups shown in figure 6.

In the $Cm'm'm'$ model the magnetic moments of Fe(1) in pyramid sites are aligned along the [010] direction. In the pyramids sharing the same O(1) atom the moments are aligned in opposite directions and the antiferromagnetic coupling is most likely facilitated by a superexchange interaction via oxygen O(1). On the other hand, in the $Cmm'm'$ Shubnikov group, magnetic moments are permitted on both Fe(1) and Fe(2) sites. However, to be consistent with the observed magnetic peak intensities and the Mössbauer data which indicate only one magnetic site, the moment on site Fe(1) has to be zero and the magnetic moment on the octahedral site Fe(2) has to be constrained to be along the *b* axis. In this model the antiferromagnetic ordering would most likely be facilitated by a superexchange interaction via oxygen O(2).

The choice of magnetic model for $Sr_4Fe_4O_{11}$ can be resolved by assigning the iron valence to the crystal sites in the structure. However, in the case of $Sr_4Fe_4O_{11}$ this is a non-trivial problem.

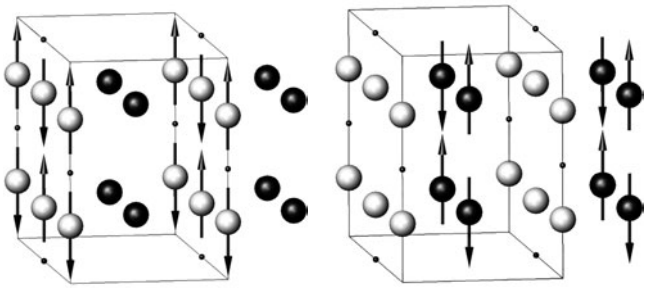

Figure 6. The $Cm'm'm'$ (left) and $Cmm'm'$ (right) models of the $Sr_4Fe_4O_{11}$ magnetic structure. The grey and black spheres represent the Fe(1) and Fe(2) iron atoms respectively. The small black spheres mark the O(1) atoms. The orthorhombic c and b axes are horizontal and vertical in the pictures respectively. The solid line outlines the unit cell.

Hodges *et al* [11] placed Fe^{4+} and Fe^{3+} ions on the pyramidal and octahedral sites respectively, based on bond strength calculations. This choice would favour the $Cmm'm'$ model. However, we find the calculations presented by Hodges *et al* [11] to be inconclusive. Hodges *et al* used the electrostatic hover model proposed by Ziółkowski [20] to calculate the bond-strength, s, and hence to assign the valence, z. The electrostatic hover model introduces a concept of standard state for ions. An ion is regarded to be in the standard state in a simple, thermodynamically stable compound (oxide). The choice of the standard state material is in some cases arbitrary [20]. By definition, the bond strength sum, Σs, around a cation in the standard state is equal exactly to its valence z. If there are n cations in non-equivalent crystallographical sites of a simple oxide, the bond strength sum over all sites equals nz. However, a sum Σs for an individual site is not necessarily equal to z [20] although Σs is not expected to substantially differ from z.

In the case of complex oxides, the individual sums Σs are expected to be different from z and the sum over all cation sites in the crystal should be greater then *the analogous sums in simple oxides taken in an equivalent number* [20] (the sum of expected valences). Therefore, for complex oxides a bond-strength sum for an individual site is not meaningful. What should be compared are the sums over all cation sites in a unit cell derived for different valence models.

Hodges *et al* [11] based their valence assignment on individual site sums Σs. Moreover, the calculations for the Fe^{3+} sites yielded Σs values which are substantially less than three. Using the data of Hodges *et al* [11], the sums of bond strengths for iron sites over the entire $Sr_4Fe_4O_{11}$ unit cell yield 26.96 and 27.72 vu for the [Fe(1) = Fe^{3+}, Fe(2) = Fe^{4+}] and [Fe(1) = Fe^{4+}, Fe(2) = Fe^{3+}] assignments respectively. The sums do not include the contribution from Sr cations, which is the same in both cases. These sums should be equal to or greater than 28 vu [20]. This gives on average 3.37 and 3.465 vu per iron site for the two models respectively. The difference between the two models is only 0.095 vu per site and the average Fe oxidation state in $Sr_4Fe_4O_{11}$ is 3.5. The absolute ionic radius used for calculations in the case of Fe^{3+} was derived assuming that the Fe^{3+} standard state is realized in haematite (Fe_2O_3). However, the absolute radius of Fe^{4+} can only be estimated due to the lack of a simple Fe^{4+} oxide [20]. It is impossible to estimate the error for the sums and therefore to disqualify one of the models.

However, there are other factors that can help in assigning the iron valence to the crystallographical sites. The chemistry and crystal structure of known Sr–Fe–O compounds yield valuable information that points to the correct valence assignment. The Fe^{4+} state is a rare state among inorganic materials and in Sr–Fe–O compounds has so far only been found to

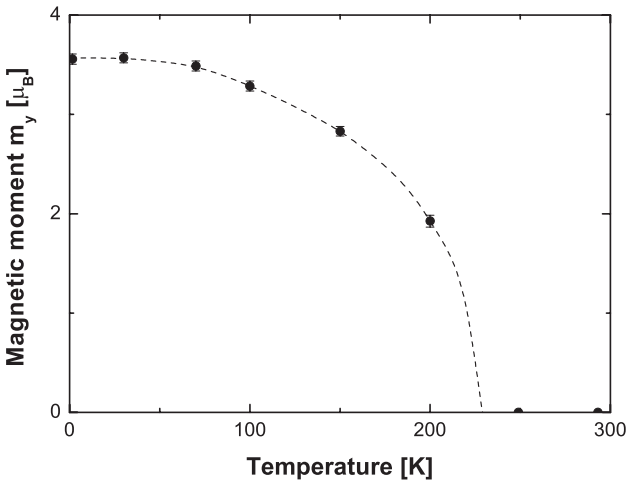

Figure 7. The refined magnetic moment values of Fe^{3+} on the Fe(1) site in $Sr_4Fe_4O_{11}$ as a function of temperature. The dashed curve is a guide for the eye.

occupy octahedral sites, e.g. $SrFeO_3$, $Sr_3Fe_2O_{7-x}$ or Sr_2FeO_4 [2, 21–23]. The five-coordinated pyramidal sites have only been observed in the $SrFeO_x$ and $Sr_3Fe_2O_{7-x}$ series. However, the appearance of pyramidal sites is always associated with the lowering of the average Fe valence below 4+. In the case of the $SrFeO_x$ series, for $SrFeO_3$, $Sr_8Fe_8O_{23}$ and $Sr_4Fe_4O_{11}$, the average iron valence values are 4+, 3.75+ and 3.5+ respectively and correspond to 0%, 25% and 50% of the iron sites being five-coordinated pyramids respectively [11]. In the case of the $Sr_3Fe_2O_{7-x}$ series, the fully oxidized $Sr_3Fe_2O_7$ structure is comprised of only octahedral sites which are being replaced by five-coordinated pyramids as the average Fe oxidation state is lowered below 4+. The other end member of this series, $Sr_3Fe_2O_6$, contains only Fe^{3+} and all Fe atoms are five coordinated [22].

The Mössbauer measurements discussed earlier indicate that Fe^{4+} in $Sr_4Fe_4O_{11}$ is in the high-spin state. Since Fe^{4+} is a $3d^4$ ion we can expect Jahn–Teller distortion to occur. Indeed the observed compression of the octahedral sites can be explained as a result of the Jahn–Teller effect. As well, it should be noted that the changes in the pyramid shape with temperature, as described above, correlate with the paramagnet–antiferromagnet transition, while the octahedral sites remain essentially unaffected.

These facts lead us to conclude that Fe^{3+} occupies the pyramidal site and that Fe^{4+} is the octahedral sites. This assignment favours the $Cm'm'm'$ magnetic model for $Sr_4Fe_4O_{11}$ and it was therefore adopted in the analysis of the experimental data presented here. However, the conclusions drawn from this particular model can be easily applied to the $Cmm'm'$ model since the Fe(1) and Fe(2) sublattices have similar topology.

The refined values of the magnetic moments on the Fe(1) atoms as determined from the $Cm'm'm'$ magnetic structure are shown in figure 7 and table 1 as a function of temperature. The magnetic moment appears to saturate below 70 K with a value of 3.55(5) μ_B. The refinement of the 1.5 K pattern in the $Cmm'm'$ model produces a similar fitting residue and a magnetic moment of 3.52(4) μ_B ($R_{wp} = 0.077$, $R_p = 0.054$, $\chi^2 = 5.234$, $R_p(-Bknd) = 0.043$). The refined moments for these two models are equal to each other within the experimental error. Rietveld plots corresponding to the two models are presented in figure 1. As these data show it is not possible to distinguish between the magnetic models from Rietveld refinement alone.

The magnetic moment of 3.55(5) μ_B at 1.5 K is unusually low for Fe^{3+} ($S = 5/2$). For comparison, the magnetic moment of Fe^{3+} reaches 4.5 μ_B at low temperatures in the case of oxygen deficient $Sr_2Fe_2O_5$ [6]. However, $Sr_2Fe_2O_5$ is an insulator and, as the oxygen content increases, the character of the electrical conductivity of $SrFeO_x$ compounds changes from insulating in $Sr_2Fe_2O_5$ to metallic in the case of $SrFeO_3$ [24]. The $SrFeO_x$ compounds from the middle of the composition range exhibit semiconducting behaviour and electrical resistivity $\rho \approx 1\ \Omega$ cm [24]. The physical properties of transition metal oxides are largely determined by the 3d electrons. The low magnetic moment value can, in principle, be explained by a partial delocallization of 3d electrons (finite electrical conductivity). However, further studies including band structure calculations are needed to fully understand this behaviour.

An estimation of the Néel point derived from neutron diffraction can be made for comparison with the magnetic susceptibility value. The three magnetic moment values closest to the ordering temperature were fitted to the equation $m(T) = \alpha(T_N - T)^\beta$ where α and T_N are fitting parameters. Due to the small number of experimental points the fit was additionally constrained by setting $\beta = 0.36$ (Heisenberg isotropic magnet). The fit yielded $T_N = 229(4)$ K with $\alpha = 0.58(1)\ \mu_B$. The calculated Néel point agrees well with the value of $T_N = 232(4)$ K determined from our magnetic susceptibility measurements.

As discussed above, the large FC susceptibility below 232 K ($\chi_{FC} > \chi_{ZFC}$, see figure 5) indicates a magnetic moment on tetravalent iron despite the apparent lack of any contribution from Fe^{4+} iron to the magnetic scattering of $Sr_4Fe_4O_{11}$. Nor, as mentioned above, do the low-temperature Mössbauer results show any short-range magnetic Fe^{4+} ordering down to 4.2 K. This unusual behaviour of the tetravalent iron moments can be understood in relation to their local environments. In figure 6, every Fe(2) site has four Fe(1) nearest neighbours. The Fe(1) moments become ordered antiferromagnetically below the Néel temperature and form pairs of magnetic moments. The Fe(2) magnetic moment could interact with the Fe(1) spins by a superexchange mechanism via the O(3) atoms. However as is evident from figure 6, the antiferromagnetic arrangement of the Fe(1) spins causes the Fe(2) moments to become frustrated. This mechanism can also explain the broadened Mössbauer line of Fe^{4+} observed at low temperatures [2, 10, 17].

4. Conclusions

$Sr_4Fe_4O_{11}$ has an orthorhombic crystal structure over the temperature range 1.5–293 K. Its crystal structure is well described by the $Cmmm$ symmetry group in the paramagnetic state. $Sr_4Fe_4O_{11}$ becomes antiferromagnetically ordered below $T_N = 232(4)$ K. The magnetic order in $Sr_4Fe_4O_{11}$ can be described using two magnetic structures based on the $Cmm'm'$ and the $Cm'm'm'$ Shubnikov groups. It is not possible to differentiate between the models on the basis of Rietveld refinements alone. The choice between the two models is possible by assigning iron valence to the particular crystallographical sites. However, examination of the general behaviour of the Sr–Fe–O compounds points towards the latter $Cm'm'm'$ space group as best describing the magnetic structure of $Sr_4Fe_4O_{11}$. The magnetic moment in the five-coordinated Fe^{3+} site saturates at 3.55(5) μ_B below 70 K. The Fe^{4+} octahedra are compressed slightly due to a Jahn–Teller effect but their shape otherwise remains essentially unchanged over the temperature range 1.5–293 K. The Fe^{4+} ions show no sign of long-range or short-range magnetic order down to 1.5 K. However, the field cooled susceptibility measurements indicate localized spins on tetravalent iron below the Néel point. The topology of the crystal lattice and the antiferromagnetic arrangement of the Fe^{3+} magnetic moments cause the tetravalent magnetic moments to become frustrated below the Néel temperature.

Acknowledgments

We acknowledge access to the E6 diffractometer at the Berlin Neutron Scattering Centre, Hahn–Meitner Institut, Berlin. This project was supported in part by US DOE Office of Science grant DE-FG02-97ER45651. Reproduction of this article, with the customary credit to the source, is permitted. SJC acknowledges renewal of his Research Fellowship from the Alexander von Humboldt Foundation during part of this work, as well as support from the Access to Major Research Facilities Program, Australian Nuclear Science and Technology Organisation.

References

[1] Shin S, Yonemura M and Ikawa H 1978 *Mater. Res. Bull.* **13** 1017
[2] Takeda Y, Kanno K, Takada T and Yamamoto O 1986 *J. Solid State Chem.* **63** 237
[3] Mizusaki J, Okayasu M, Yamaguchi S and Fueki K 1992 *J. Solid State Chem.* **99** 166
[4] Grenier J C, Ea N, Pouchard M and Hagenmuller P 1985 *J. Solid State Chem.* **58** 243
[5] Schmidt M and Campbell S J 2002 *J. Phys. Chem. Solids* **63** 2085
[6] Schmidt M and Campbell S J 2001 *J. Solid State Chem.* **156** 292
[7] Schmidt M W 2001 Phase formation and structural transformation of strontium ferrite $SrFeO_x$ *PhD Thesis* The Australian National University, Canberra
[8] Steele B C H 1988 *British Ceramic Proc.* vol 43 (Stoke-on-Trent: Institute of Ceramics) p 163
[9] Steele B C H 1996 *Curr. Opin. Solid State Mater. Sci.* **1** 684
[10] Takano M, Okita T, Nakayama N, Bando Y, Takeda Y, Yamamoto O and Goodenough J B 1988 *J. Solid State Chem.* **73** 140
[11] Hodges J P, Short S, Jorgensen J D, Xiong X, Dabrowski B, Mini S M and Kimball C W 2000 *J. Solid State Chem.* **151** 190
[12] Zhao Y M, Yang X J, Zheng Y F, Li D L and Chen S Y 2000 *Solid State Commun.* **115** 365
[13] Zhao Y M, Mahendiran R, Nguyen N, Raveau B and Yao R H 2001 *Phys. Rev.* B **64** 024414
[14] Tofield B C, Greaves C and Fender B E F 1975 *Mater. Res. Bull.* **10** 737
[15] Schmidt M 2000 *J. Phys. Chem. Solids* **61** 1363
[16] Larson A C and Von Drele R B 1994 GSAS general structure analysis system *Los Alamos National Laboratory Technical Report* LAUR 86-748
[17] Gibb T C 1985 *J. Chem. Soc. Dalton Trans.* 1455
[18] Fournès L, Potin Y, Grenier J C, Demazeau G and Pouchard M 1987 *Solid State Commun.* **62** 239
[19] Gütlich P 1975 *Mössbauer Spectroscopy* (Berlin: Springer) p 53
[20] Ziółkowski J 1985 *J. Solid State Chem.* **57** 269
[21] Dann S E, Weller M T and Currie D B 1991 *J. Solid State Chem.* **92** 237
[22] Dann S E, Weller M T and Currie D B 1992 *J. Solid State Chem.* **97** 179
[23] Dann S E, Weller M T, Currie D B, Thomas M F and Al-Rawwas A D 1993 *J. Mater. Chem.* **3** 1231
[24] MacChesney J B, Sherwood R C and Potter J F 1965 *J. Chem. Phys.* **43** 1907